Progress In Electromagnetics Research M, Vol. 93, 197–207, 2020

Research on Active Disturbance Rejection Control of Hybrid Excitation Magnetic Suspension Switched Reluctance Motor Considering Noise

Yonghong Huang*, Libin Yan, Fan Yang, and Wenjun Zeng

Abstract—The bearingless switched reluctance motor system based on active disturbance rejection control has good anti-interference performance and robustness, but it is easy to lose stability due to the influence of measurement noise in actual engineering. The main reason for the sensitivity of active disturbance rejection control to noise lies in the noise amplification of its extended state observer. To solve this problem, a novel reduced-order extended state observer based on predictive linear tracking differentiator is proposed. First, the general form of the observer is given, and then active disturbance rejection controller is designed based on suspension system of the hybrid excitation bearingless switched reluctance motor. The suspension force is used as the hysteresis loop to eliminate the estimation of the disturbance feedforward gain, and the stability of the control system is analyzed by Lyapunov equation. Finally, the simulation comparison is conducted through Matlab. The results show that this method can effectively suppress the influence of measurement noise and reduce the error of disturbance estimation when the observer is in a low bandwidth.

1. INTRODUCTION

Bearingless Switched Reluctance Motor [1] (BSRM) combines the characteristics of magnetic bearing and switched reluctance motor which has the advantages of high output power, no mechanical wear, and high speed adaptability [2, 3]. BSRM has broad application prospects in special fields such as flywheel battery, aerospace, and biomedicine [4, 5].

The shortcomings of strong coupling and nonlinearity of BSRM [6] lead to the difficulty of system modeling and control, which seriously limits its development and application. Therefore, in order to improve the torque and suspension performance of BSRM, [7] proposed a minimum flux control strategy by analyzing the influence of winding flux on radial suspension force and torque, which reduced torque ripple and stator vibration.[8] reduced rotor eccentric displacement based on adaptive fuzzy PID control. Through the reversibility analysis of the model, [9] constructed direct or modified inverse to realize the high-performance decoupling control. The above control strategies have their own advantages, but their ability to deal with uncertain factors is limited, or their design is difficult to achieve. To further improve the control performance, this paper carries out a research on the control system of hybrid excitation bearingless switch reluctance motor based on active disturbance rejection control.

Active Disturbance Rejection Control (ADRC) is a novel control strategy proposed by Han [10]. Gao [11] introduced it into engineering applications through the concept of bandwidth. Guo and Zhao [12-13] systematically demonstrated the stability of auto disturbance rejection control. ADRC has been widely used in gyroscope [14], aircraft attitude [15], and servo system control [16, 17]. However, the core of ADRC is Extended State Observer (ESO). High frequency measurement noise will inevitably exist in

Received 9 April 2020, Accepted 12 June 2020, Scheduled 29 June 2020
* Corresponding author: Yonghong Huang (hyh@ujs.edu.cn).
The authors are with the School of Electrical and Information Engineering, Jiangsu University, Zhenjiang 212013, China.

the actual project in order to quickly track the disturbance, and ESO will amplify the noise to make the actuator bear the high frequency vibration, and then cause damage to the device. To reduce the observer feedback gain, Tian [18] proposed Reduced-order Extended State Observer (RESO) by combining the idea of reduced-order observer with ESO. However, noise still influenced the observer. Although reducing the bandwidth can effectively reduce the impact of noise, it also reduces the observation performance of the observer. Therefore, the comprehensive consideration of the noise tolerance and observation performance of ESO still has research value.

In this paper, 12/14 Hybrid Excitation Bearingless Switched Reluctance Motor (HEBSRM) is taken as the research object. HEBSRM realizes the decoupling of torque and suspension force on the natural structure. The research on torque system by domestic and foreign scholars was relatively mature [19–22]. Therefore, the control of the research object should consider the model uncertainty, coupling between degrees of freedom, and external disturbance of the suspension system. In order to improve the response of the control system and omit the estimation of the disturbance feedforward gain, direct suspension force control is used instead of current hysteresis control. First introduce the structure and suspension principle of HEBSRM, and derive its mathematical model. Then a Novel Reduced-order Extended State Observer (NRESO) based on Predictor Linear Tracking Differentiator (PLTD) [23] is designed, and the design of ADRC is further completed. Finally, simulation proves that the novel observer has more advantages in noise tolerance and disturbance observation, which effectively reduces rotor displacement and improves the robustness of the system.

2. STRUCTURE AND MATHEMATICAL MODEL OF HEBSRM

The structure of HEBSRM is shown in Fig. 1. The suspension system and torque system adopt a stator structure with a mixture of wide and narrow poles, which are sequentially spaced into suspension and torque poles, and a magnetic isolation aluminum ring is embedded between the suspension and torque poles to achieve the natural decoupling of suspension force and torque.

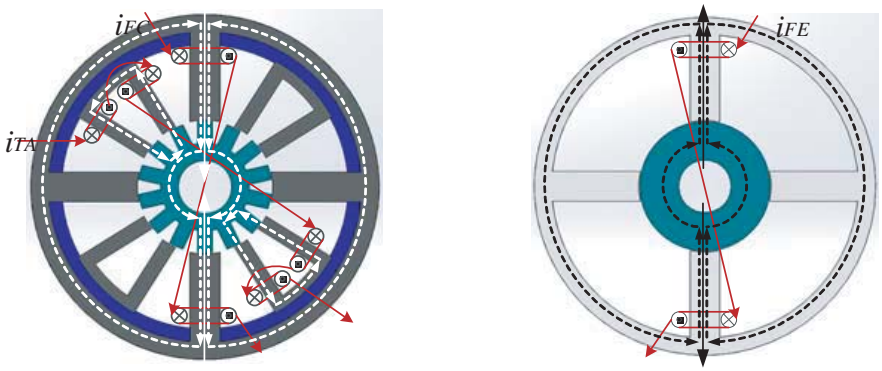

Figure 1. Structure of HEBSRM.

The main parameters of the motor used in this article are shown in Table 1.

To simplify the analysis, the motor is set to an ideal state without considering hysteresis and eddy current loss. When the system is in equilibrium, the equivalent magnetic circuit can be obtained as shown in Fig. 2.

In Fig. 2, N is the number of turns of the suspension winding; i_x, i_y are the suspension control currents; F_{pm} is the flux force of the permanent magnet ring. R represents the reluctance between the air gaps, and their values are shown as follows

$$\begin{cases} R_{x1+} = R_{x1-} = \dfrac{l - x_0}{\mu_0 S}, & R_{x2+} = R_{x2-} = \dfrac{l + x_0}{\mu_0 S} \\ R_{y1+} = R_{y1-} = \dfrac{l - y_0}{\mu_0 S}, & R_{y2+} = R_{y2-} = \dfrac{l + y_0}{\mu_0 S} \end{cases} \tag{1}$$

Table 1. The main parameters of the motor.

Parameters	Value	Parameters	Value
Suspension stator outer diameter (mm)	15	Torque stator outer diameter (mm)	124
Suspension Stator inner diameter (mm)	65	Torque stator outer diameter (mm)	65
Rotor inner diameter (mm)	64	Permanent magnet ring outer diameter (mm)	150
Rotor inner diameter (mm)	26	Permanent magnet ring inner diameter (mm)	132
Pole-arc of suspension (deg)	12.85	Thickness of permanent magnet ring (mm)	1.5
Pole-arc of Torue (deg)	25.7	Air-gap length (mm)	0.5

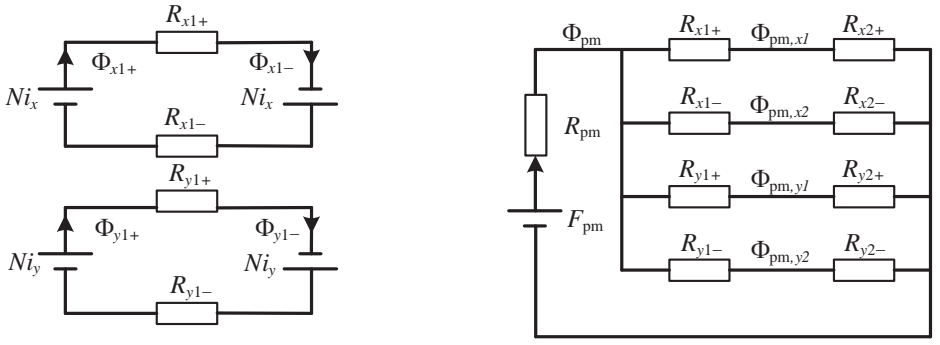

(a) Control equivalent magnetic circuit (b) Bias equivalent magnetic circuit

Figure 2. Equivalent magnetic circuit diagram of suspension system.

where l is the length of the air gap when the rotor is in a balanced position; x_0, y_0 are the radial offset of the rotor, respectively; μ_0 is the vacuum permeability; S is the effective cross-sectional area of the magnetic circuit of the suspension system. According to Fig. 2, the formulas for the magnetic flux Φ in each direction can be expressed as

$$\begin{cases} \Phi_{x1+} = \Phi_{x1-} = \dfrac{2Ni_x}{R_{x1+} + R_{x1-}} \\ \Phi_{y1+} = \Phi_{y1-} = \dfrac{2Ni_y}{R_{y1+} + R_{yu1-}} \end{cases} \tag{2}$$

$$\begin{cases} \Phi_{\mathrm{pm},x1} = \dfrac{F_{\mathrm{pm}} \cdot R_{\mathrm{pm}}}{R_{x1+} + R_{x2+} + R_{\mathrm{pm}}} \\ \Phi_{\mathrm{pm},x2} = \dfrac{F_{\mathrm{pm}} \cdot R_{\mathrm{pm}}}{R_{x1-} + R_{x2-} + R_{\mathrm{pm}}} \\ \Phi_{\mathrm{pm},y1} = \dfrac{F_{\mathrm{pm}} \cdot R_{\mathrm{pm}}}{R_{y1+} + R_{y2+} + R_{\mathrm{pm}}} \\ \Phi_{\mathrm{pm},y2} = \dfrac{F_{\mathrm{pm}} \cdot R_{\mathrm{pm}}}{R_{y1-} + R_{y2-} + R_{\mathrm{pm}}} \end{cases} \tag{3}$$

$\Phi_{\mathrm{pm}} = \Phi_{\mathrm{pm},x1} + \Phi_{\mathrm{pm},x2} + \Phi_{\mathrm{pm},y1} + \Phi_{\mathrm{pm},y2}$, thus, an analysis of the suspension force F_x in the x-axis direction, for example, can be obtained from the equivalent magnetic circuit diagram.

$$\begin{cases} \Phi_{x1+} = \Phi_{x1-} = (\Phi_{x1+} + \Phi_{\mathrm{pm}})^2 + (\Phi_{x1-} - \Phi_{\mathrm{pm}})^2 \\ \Phi_{x2+} = \Phi_{x2-} = (\Phi_{x2+} + \Phi_{\mathrm{pm}})^2 + (\Phi_{x2-} - \Phi_{\mathrm{pm}})^2 \end{cases} \tag{4}$$

$$F_x = \frac{\Phi_{x1+}^2}{2\mu_0 S} - \frac{\Phi_{x1-}^2}{2\mu_0 S} \tag{5}$$

By linearizing Equation (5), the linearized equation of the rotor near the equilibrium position can

be obtained

$$F_x = \frac{\partial F_x}{\partial x_0}\bigg|_{\substack{i_x=0\\x_0=0\\y_0=0}} x_0 + \frac{\partial F_x}{\partial i_x}\bigg|_{\substack{i_x=0\\x_0=0\\y_0=0}} i_x = k_i i + k_x x \tag{6}$$

3. DESIGN OF ACTIVE DISTURBANCE REJECTION CONTROLLER

There are parameter uncertainties, coupling effects, and external disturbances in the suspension part of the HEBSRM, so the use of decentralized PID control is not conducive to good control performance. ADRC can treat the above factors as comprehensive disturbances and compensate system, so better control performance can be obtained by using ADRC. By linearizing Equation (2), the linearized equation of the rotor near the equilibrium position is

$$F_x = k_i i + k_x x \tag{7}$$

where k_i is the current stiffness, k_x the displacement stiffness, i the input current, x the displacement, and F_x the single degree of freedom suspension force on the x-axis. The comprehensive disturbance is defined as

$$f = g\left(\dot{x}, x, t\right) + d + \left(b - \hat{b}\right) u \tag{8}$$

where g is the internal uncertain dynamics of the system, d the external perturbation, $\hat{b}$ the estimate of b, and u the input current i.

Let $x = x_1$, $\dot{x} = x_2$, the total disturbances are expanded to a new state variable x_3 and $\dot{x}_3 = \omega$, while considering the effect of noise, the state space equation of this degree of freedom can be:

$$\begin{cases} \dot{\mathbf{x}} = \mathbf{A}\mathbf{x} + \mathbf{B}\mathbf{U} \\ \mathbf{y} = \mathbf{C}\mathbf{x} + \mathrm{v} \end{cases} \tag{9}$$

where $\mathbf{A} = \begin{pmatrix} 0 & 1 & 0 \\ 0 & 0 & 1 \\ 0 & 0 & 0 \end{pmatrix}$, $\mathbf{B} = \begin{pmatrix} 0 & 0 \\ \hat{b} & 0 \\ 0 & 1 \end{pmatrix}$, $\mathbf{C} = \begin{pmatrix} 1 \\ 0 \\ 0 \end{pmatrix}^T$, $\mathbf{U} = \begin{pmatrix} u & \omega \end{pmatrix}^T$, $\mathbf{x} = \begin{pmatrix} x_1 & x_2 & x_3 \end{pmatrix}^T$.

For Equation (5), ignoring its noise effects for the time being, the following can be obtained.

$$rank\begin{pmatrix} \lambda_i \mathbf{I} - \mathbf{A} & \mathbf{B} \end{pmatrix} = \begin{pmatrix} 0 & -1 & 0 & 0 & 0 \\ 0 & 0 & -1 & \hat{b} & 0 \\ 0 & 0 & 0 & 0 & 1 \end{pmatrix} = 3 \tag{10}$$

$$rank\begin{pmatrix} \lambda_i \mathbf{I} - \mathbf{A} \\ \mathbf{C} \end{pmatrix} = \begin{pmatrix} 0 & -1 & 0 \\ 0 & 0 & -1 \\ 0 & 0 & 0 \\ 1 & 0 & 0 \end{pmatrix} = 3 \tag{11}$$

According to the PHB criterion, the system can be controlled and observed. When state feedback is achieved using observer estimates, the observer design can be done independently.

3.1. Design of Reduced-Order Extended State Observer

Achieving accurate estimates of comprehensive disturbances is the key to designing ADRC. ESO is very sensitive to noise. The ESO proposed in [10], due to its large feedback gain under the relative bandwidth, will significantly reduce the bandwidth to reduce the impact of noise, which causes a serious loss of its disturbance estimation capability. For this problem, the special form proposed in [13] will be

adopted, which reduces the feedback gain at the same bandwidth. The structure of item is shown in Equation (8).

$$\begin{cases} e_o = r^2 (x_1 - \hat{x}_1) \\ \dot{\hat{x}}_1 = \hat{x}_2 + \dfrac{k_1}{r} fal_1 (e_o) \\ \dot{\hat{x}}_2 = \hat{x}_3 + \hat{b}u + k_2 fal_2 (e_o) \\ \dot{\hat{x}}_3 = r k_3 fal_3 (e_o) \end{cases} \tag{12}$$

where $r > 0$ is the feedback gain, and $\hat{x}_i$ is the estimate of x_i, $i = 1, 2, 3$. In addition

$$fal (e_o, \alpha_i, \delta) = \begin{cases} \dfrac{e_o}{\delta_i^{1-\alpha_i}}, \ |e_o| \le \delta \\ |e_o|^{\alpha_i} \operatorname{sgn} (e_o), \ |e_o| > \delta \end{cases}, \quad \alpha_i (i = 1, 2, 3) = i\alpha_1 - (i-1), \text{ let } \delta = 1.$$

k_1, k_2, k_3 in Equation (8) are the constants that make the following matrix $\mathbf{K}$ to satisfy Hurwitz.

$$\mathbf{K} = \begin{pmatrix} -k_1 & 1 & 0 \\ -k_2 & 0 & 1 \\ -k_3 & 0 & 0 \end{pmatrix} \tag{13}$$

Since the differential signal of displacement is also measurable, in order to further reduce the influence of noise, the system is corrected according to the design in the literature [18]. Let $\dot{x} = z_1$, $f = z_2$, then the new state space equation can be obtained.

$$\begin{cases} \dot{z}_1 = \hat{b}u + z_2 \\ \dot{z}_2 = \omega \end{cases} \tag{14}$$

For the above system, the RESO is designed as follows

$$\begin{cases} e_{ro} = r (z_1 - \hat{z}_1) \\ \dot{\hat{z}}_1 = \hat{z}_2 + \hat{b}u + k_{r1} fal_{r1} (e_{ro}) \\ \dot{\hat{z}}_2 = r k_{r2} fal_{r2} (e_{ro}) \end{cases} \tag{15}$$

To further enhance the disturbance observation ability, the observation of the expanded state is redesigned according to the nonlinear PID of [24]

$$\hat{f} = r k_{r2} \int fal_{r2} (e_{ro}) + k_{r1} fal_{r1} (e_{ro}) \tag{16}$$

Different from [24], Equation (12) only uses the nonlinear PI of the observation error for estimation, which reduces the noise amplification that may be caused by the differential term.

The above study reduces the observer feedback gain, but does not process the noise signal. Since the observer design adopts the form of PI, and the integration term has a good suppression effect on high frequency noise, only the proportional term needs to be denoised. Excessive filtering of the signal will cause serious phase loss. PLTD is adopted to reduce phase loss, and its structure is shown in Equation (13).

$$\begin{cases} \bar{v}_1 = v_1 + k_{1T} h v_2 \\ \dot{v}_1 = v_2 \\ \dot{v}_2 = -R^2 (a_1 (\bar{v}_1 - v_0) + a_2 v_2 / R) \end{cases} \tag{17}$$

where v_0 is the reference signal; v_1 and v_2 are the tracking value and its differential; R and a are the corresponding gains; k_{1T} is the iteration step; h is the integration step. Therefore, the final state observer is designed as

$$\begin{cases} e_{ro} = r (x_2 - \hat{x}_2) \\ \dot{\hat{z}}_1 = \hat{z}_2 + \hat{b}u + k_{r1} fal_{r1} (e_{ro}) \\ \dot{\hat{z}}_2 = r k_{r2} fal_{r2} (e_{ro}) \\ v_0 = fal_{r2} (e_{ro}) \\ \dot{v}_1 = v_2 \\ \dot{v}_2 = -R^2 (a_1 (\bar{v}_1 - v_0) + a_2 v_2 / R) \\ \bar{v}_1 = v_1 + k_{t1} h v_2 \\ \hat{f} = r k_{r2} \int fal_{r2} (e_{ro}) + k_{r1} \bar{v}_1 \end{cases} \tag{18}$$

Denoising a single item for the observer greatly reduces the amount of calculation and phase loss, and reduces the chattering phenomenon in NRESO to a certain extent by using PLTD.

3.2. Design of Feedback Control Rate

The conventional suspension control generally adopts position and current loop. In order to speed up the response of the system, the direct suspension force control is adopted in this paper. The suspension force is used as a hysteresis loop instead of a current loop. The block diagram of direct suspension force control is shown in Fig. 3.

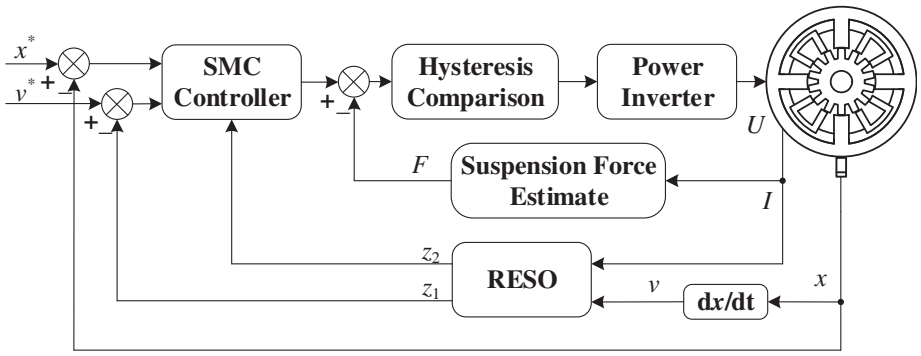

Figure 3. Block diagram of direct suspension force control.

Let $F_x = m\ddot{x} = u_0$, and redesign the system state equation as follows

$$\begin{cases} \dot{x}_1 = x_2 \\ \dot{x}_2 = \dfrac{1}{m}(u_0 + f) \\ y = x_1 \end{cases} \tag{19}$$

Define x^* as the reference displacement, $e_1 = x^* - x_1$, and select the sliding surface as follows

$$s = k_s e_1 + \dot{e}_1 \tag{20}$$

The design of feedback control rate is

$$u_0 = -\hat{f} - mk_s\dot{x}_1 + mq\,|s|^{\alpha_s}\,\mathrm{sgn}(s) \tag{21}$$

where m is the rotor mass, $q > 0$, $1 > \alpha_s > 0$. Through direct suspension force control, the system omits the estimation of the disturbance feedforward gain required by conventional ADRC and reduces the controller's dependence on the system model.

4. PROOF OF STABILITY

The PLTD used in the observer design was analyzed in [25] in the frequency domain. The results show that it has good filtering and tracking capabilities, so this section will analyze the rest of the design. Consider an ideal situation where both the system state variable x and its derivatives are bounded, and there is

$$f + \left|\frac{\partial f}{\partial t}\right| < M \tag{22}$$

According to [13], Equation (11) converges. The equation of state for Equation (11) is equivalent to the nonlinear differential equation.

$$\dot{\hat{z}}_1 = \hat{b}u + k_{r1} fal_{r1}(e_{ro}) + rk_{r2}\int fal_{r2}(e_{ro}) \tag{23}$$

Take Equation (12) into Equation (19) to get

$$\dot{\hat{z}}_1 = \hat{b}u + \hat{f} \tag{24}$$

Since Equation (9) converges, it is known that $\dot{\hat{z}}_1 \to \dot{z}_1$, then $\hat{f} \to z_2 = f$. Therefore, when the system state variables and their derivatives are bounded, the observer mentioned in this paper converges. Let $f - \hat{f} = \tilde{f}$, and from the convergence of the observer, $|\tilde{f}| \leq \eta$ can be obtained. The Lyapunov function is chosen as

$$V = \frac{1}{2}s^2 \tag{25}$$

Derive Equation (16)

$$\dot{s} = -k_s\dot{x}_1 - \frac{1}{m}(u_0 + f) \tag{26}$$

where $k_s > 0$. Derive Equation (21) and substitute Equation (22) into it.

$$\dot{V} = s\left[\frac{1}{m}\left(\hat{f} - f\right) - q\,|s|^{\alpha_s}\operatorname{sgn}(s)\right] = \frac{-\tilde{f}}{m}s - q\,|s|^{\alpha_s}\,|s| \leq \frac{\eta}{m}s - q\,|s|^{\alpha_s}\,|s| \leq |s|\left(\frac{\eta}{m} - q\,|s|^{\alpha_s}\right) \tag{27}$$

when $t \to \infty$, $|s| \leq (\frac{\eta}{mq})^{\frac{1}{\alpha}}$ [25]. Thus, $\dot{V} \leq 0$ and the stability of sliding mode can be proved.

5. SIMULATION VERIFICATION AND ANALYSIS

To verify the effectiveness of the proposed control strategy in HEBSRM suspension system, NRESO is compared with ESO and DOB in the literature based on MATLAB environment under the framework of ADRC. The simulation parameters are shown in Table 2.

Table 2. Simulation parameters of control system.

Parameters	Value
m(kg)	5
k_i(N/A)	40
k_x(N/m)	-40000
k_s	200
α_s	0.5
q	20
$R(\Omega)$	0.4
L(H)	0.0028

In the simulation, the parameters of the controller are constant, and the same observer parameters $r = 2000$, $n = 1000$, $h = 1e-5$, $k_{1T} = 100$ are selected. The external disturbance is set as $d(t) = 10(1 - e^{-500(t-0.1)})$. The Gaussian white noise with a sampling period of 0.0005 s, mean value of 0, and variance of $1e-14$ is introduced. Compare the performances of the observer with or without noise.

The performance comparison of the observers before and after adding noise is shown in Fig. 4. The NRESO proposed in this paper is obviously superior to the RESO and ESO in disturbance observation performance, but due to the lack of differential link, the phase is not optimized, and the observation performance has a certain loss. When Gaussian white noise is added, DOB is too sensitive to noise to be used directly in a noise-inclusive system. However, the NRESO still has good observation performance, which effectively compensates the disturbance estimation error of ESO at low bandwidth.

The comparison of current and displacement with the above-mentioned observers is shown in Fig. 5 and Fig. 6. The control system with ESO and DOB has lost stability and has large high-frequency

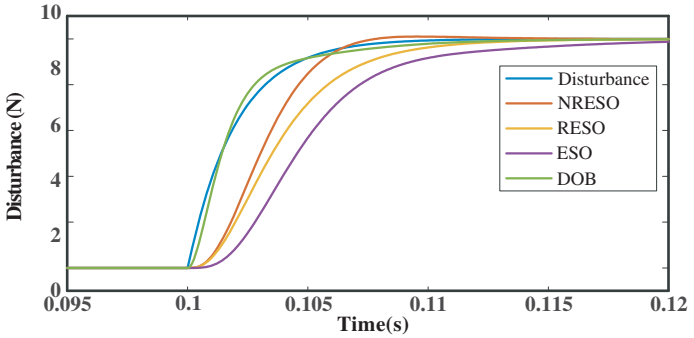

(a) With noise

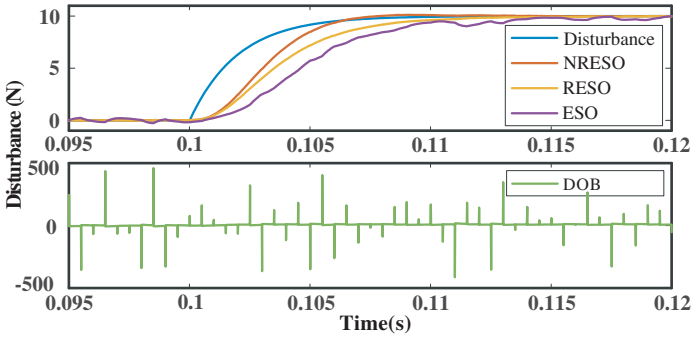

(b) Without noise

Figure 4. Results of observers performance comparison.

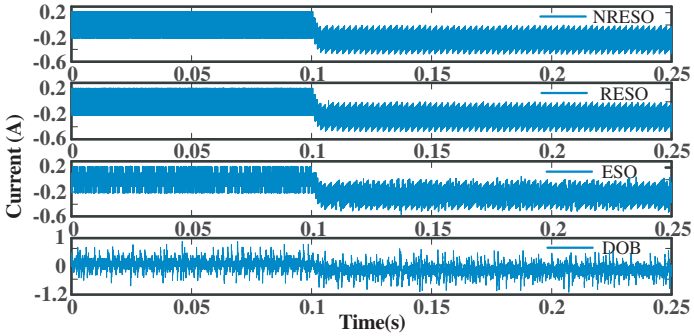

Figure 5. Comparison of current under noise.

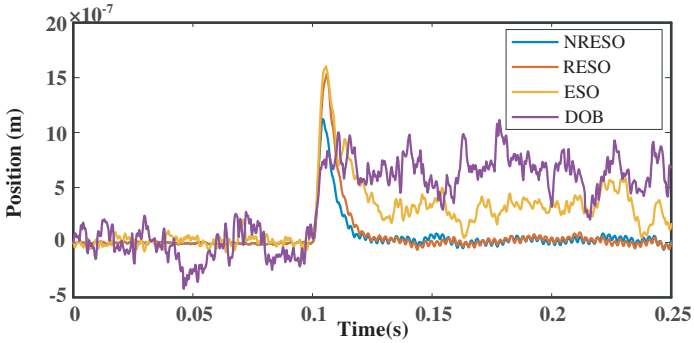

Figure 6. Comparison of displacement under noise.

chatter. The ADRC based on RESO and NRESO remains stable under noise conditions, and the displacement of the latter is reduced by about 30% compared with the former, which enhances the disturbance rejection performance of the system.

To further verify the performance of the control strategy proposed in this paper, on the basis of the above operating conditions, the robustness of the motor parameter under perturbation is tested. The mass and winding resistance of the motor change little in the running state, so the parameter perturbations of +20% and −20% for remaining parameters are increased, respectively. The simulation results are shown in Fig. 7.

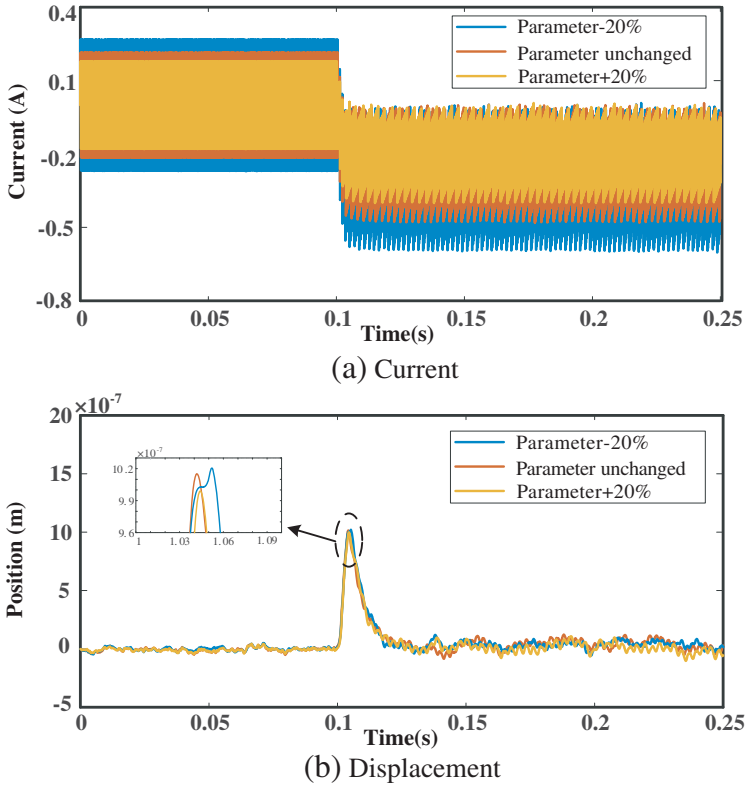

Figure 7. Comparison of current and displacement under parameter perturbation.

The comparisons of current and displacement of suspension system under parameter perturbation are shown in Fig. 7, respectively. Due to the difference of inductance and current stiffness, the current changes greatly, but there is only a slight difference for the rotor offset after disturbance, and the suspension system remains stable, which verifies the robustness of the system.

6. CONCLUSION

In this paper, the ADRC problem of HEBSRM suspension system is studied. For the high frequency noise, a reduced-order extended state observer based on the predictor linear tracking differential is designed, and active disturbance rejection controller is built on this basis. The introduction of direct suspension force control in the closed loop avoids the estimation of disturbance feedforward gain and enhances the reliability of the system. The simulation results show that compared with the general extended state observer and disturbance observer, this method has the characteristics of suppressing noise pollution, effectively reducing the error of disturbance estimation, improving the disturbance rejection performance of the system, and enhancing the robustness of the system.

ACKNOWLEDGMENT

This work was supported in part by the National Natural Science Foundation of China under Project 51707082 and Project 51877101, by Natural Science Foundation of Jiangsu Province of China (Grants No. BK20170546), and by the Priority Academic Program Development of Jiangsu Higher Education Institutions (PAPD).

REFERENCES

1. Takemoto, M., A. Chiba, H. Akagi, et al., "Radial force and torque of a bearingless switched reluctance motor operating in a region of magnetic saturation," *IEEE Transactions on Industry Applications*, Vol. 40, No. 1, 103–112, 2004.
2. Sun, Y., F. Yu, Y. Yuan, Z. Huang, Y. Huang, and Z. Zhu, "A hybrid double Stator bearingless switched reluctance motor," *Transactions of China Electrotechnical Society* Vol. 34, No. 1, 1–10, 2019.
3. Wang, H. and F. Li, "Design consideration and characteristic investigation of modular permanent magnet bearingless switched reluctance motor," *IEEE Transactions on Industrial Electronics*, Vol. 67, No. 6, 4326–4337, 2020.
4. Yuan, Y., Y. Huang, Q. Xiang, et al., "Mathematical modeling and control for a single winding bearingless flywheel motor in electric/suspension mode," *Journal of Electrical Engineering & Technology*, Vol. 13, No. 5, 1935–1944, 2018.
5. Huang, Y., F. Huang, Y. Yuan, F. Yang, and K. Xie, "Design and analysis of a novel nearingless segmented switched reluctance motor," *IEEE Access*, Vol. 7, 94342–94349, 2019.
6. Sun, Y., Y. Yuan, Y. Huang, W. Zhang, and L Liu, "Development of the bearingless switched reluctance motor and its key technologies," *Transactions of China Electrotechnical Society*, Vol. 30, No. 22, 1–8, 2015.
7. Yang, Y., Z. Deng, G. Yang, X. Cao, and Q. Zhang, "A control strategy for bearingless switched reluctance motors," *IEEE Transactions on Power Electronics*, Vol. 25, No. 11 2807–2819, 2010.
8. He, Y., Y. Tang, D. Lee, and J. Ahn, "Suspending control scheme of 8/10 bearingless SRM based on adaptive fuzzy PID controller," *Chinese Journal of Electrical Engineering*, Vol. 2, No. 2, 60–67, 2016.
9. Zhu, Z. and Y. Sun, "Universal decoupling control for bearingless switched reluctance motors based on the direct-inverse and correct-inverse system," *Proceedings of the CSEE*, Vol. 34, No. 33, 5902–5909, 2014.
10. Han, J., "From PID to active disturbance rejection control," *IEEE Transactions on Industrial Electronics*, Vol. 56, No. 3, 900–906, 2009.
11. Gao, Z., "Scaling and bandwidth-parameterization based controller tuning," *Proceedings of the 2003 American Control Conference*, 4989–4996, Denver, CO, USA, 2003.
12. Guo, B. and Z. Zhao, "On the convergence of an extended state observer for nonlinear systems with uncertainty," *Systems & Control Letters*, Vol. 60, No. 6, 420–430, 2011.
13. Zhao, Z. and B. Guo, "A nonlinear extended state observer based on fractional power functions," *Automatica*, Vol. 81, 286–296, 2017.
14. Dong, L., Q. Zheng, and Z. Gao, "On control system design for the conventional mode of operation of vibrational gyroscopes," *IEEE Sensors Journal*, Vol. 8, No. 11, 1871–1878, 2008.
15. Mauricio, A., C. Luigi, P. Carlos, C. Enrico, and N. Carlo, "UAV quadrotor attitude control: An ADRC-EMC combined approach," *Control Engineering Practice*, Vol. 84, 13–22, 2019.
16. Liu, C., G. Luo, Z. Chen, W. Tu, and C. Qiu, "A linear ADRC-based robust high-dynamic double-loop servo system for aircraft electro-mechanical actuators," *Chinese Journal of Aeronautics*, Vol. 32, No. 9, 2174–2187, 2019.
17. Tian, C., P. Yan, and Z. Zhang, "Inter-sample output predictor based sampled-data ADRC supporting high precision control of VCM servo systems," *Control Engineering Practice*, Vol. 85, 138–148, 2019.

18. Tian, G., "Reduced-order extended state observer and frequency response analysis," Cleveland State University, Cleveland, 2007.
19. Chen, H., H. Yang, Y. Chen, and H. Iu, "Reliability assessment of the switched reluctance motor drive under single switch chopping strategy," *IEEE Transactions on Power Electronics*, Vol. 31, No. 3, 2395–2408, 2016.
20. Moron, C., A. Garcia, E. Tremps, and J. Somolinos, "Torque control of switched reluctance motors," *IEEE Transactions on Magnetics*, Vol. 48, No. 4, 1661–1664, 2012.
21. Jakobsen, U., K. Lu, P. O. Rasmussen, D. Lee, and J. Ahn, "Sensorless control of low-cost single-phase hybrid switched reluctance motor drive," *IEEE Transactions on Industry Applications*, Vol. 51, No. 3, 2381–2387, 2015.
22. Li, X. and P. Shamsi, "Inductance surface learning for model predictive current control of switched reluctance motors," *IEEE Transactions on Transportation Electrification*, Vol. 1, No. 3, 287–297, 2015.
23. Zhang, M., L. Yang, Y. Hou, Y. Shi, and G. Zuo, "Improved linear active disturbance rejection controller with Denoising Performance," *Journal of Astronautics*, Vol. 40, No. 7, 803–810, 2019.
24. Yao, S. and G. Gao, and Z. Gao, "Bandwidth parameterized disturbance observer composite sliding mode coordination control for closed chain mechanisms," *Control Theory & Applications*, 1–7.
25. Li, P., J. Ma, and Z. Zheng, "Sliding mode control approach based on nonlinear integrator," *Control Theory & Applications*, Vol. 28, No. 5, 619–624, 2011.